

Polymer crystal-melt interfaces and nucleation in polyethylene

Scott T. Milner

Department of Chemical Engineering

The Pennsylvania State University

University Park, PA 16802

March 9, 2022

Abstract

Kinetic barriers cause polymers to crystallize incompletely, into nanoscale lamellae interleaved with amorphous regions. As a result, crystalline polymers are full of crystal-melt interfaces, which dominate their physical properties. The longstanding theoretical challenge to understand these interfaces has new relevance, because of accumulating evidence that polymer crystals often nucleate via a metastable, partially ordered “rotator” phase. To test this idea requires a theory of the bulk and interfacial free energies of the critical nucleus. We present a new approach to the crystal-melt interface, which represents the amorphous region as a grafted brush of loops in a self-consistent pressure field. We combine this theory with estimates of bulk free energy differences, to calculate nucleation barriers and rates via rotator versus crystal nuclei for polyethylene. We find rotator-phase nucleation is indeed favored throughout the temperature range where nucleation is observed. Our methods can be extended to other polymers.

Introduction

Polymer chain connectivity has an enormous influence on the structure of crystals and the kinetics of crystallization. To begin with, crystallizable homopolymers are universally observed to be “semicrystalline” — that is, to consist of closely spaced lamellar crystallites of nanoscale thickness, separated by amorphous uncrystallized regions of comparable thickness.¹ (See Fig. 1.)

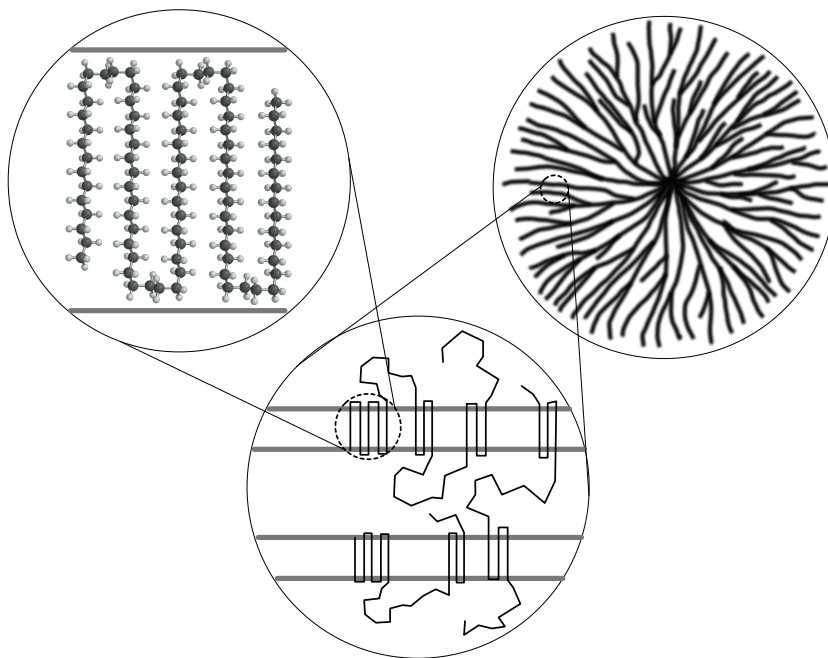


Figure 1: “Multiscale” schematic of semicrystalline polymers. Chain-folded crystalline lamellae of thickness $\sim 10\text{nm}$ lie adjacent to amorphous regions of comparable thickness; these are organized into micron-sized spherulites, consisting of lamellae emanating in all directions from a central nucleation site.

This crystalline lamellar structure is observed even though the lowest free energy state of a crystallizable homopolymer is certainly an extended-chain crystal, with no amorphous regions. In such a crystal, which can be grown only by heroic measures, the long polymer molecules adopt a regular packing of linear conformations (all-trans, or helices) in which the chains are all parallel.

The reason polymers routinely crystallize in a lamellar morphology is kinetic: the

time for chains in the random-coil configurations of a melt to find their way to a fully extended state is so long, that faster modes of crystal growth prevail.¹ That faster mode is lateral growth of a crystal nucleus, by incorporating nearby chain segments as they are encountered by the growth front. Only a portion of long chains will be “combed out” to parallel conformations as the lamella grows past.

The result of this lamellar growth is that on either face of the lamella, all the snarls and tangles that were combed out from the crystallized region accumulate in as yet uncrystallized material. These accumulated entanglements, as well as the limited space between adjacent lamellae, eventually inhibit further crystallization.

As a consequence, crystallizable polymers are full of crystal-melt interface. This has dramatic consequences for the material properties. The high degree of plastic deformation of solid polymers depends on the existence of the amorphous regions and their connectivity through chains to adjacent lamellae.

If the chains are so short that there are insufficient “tie chains” between lamellae, the material becomes brittle.^{2,3} (For very short unentangled polymer molecules, the above kinetic considerations, leading to lamellar crystals with amorphous material sandwiched between, no longer apply. Polyethylene of less than 50 carbons or so is alkane wax, and crystallizes completely; equilibrium crystal-melt interfaces for such short chains consist mostly of chain ends, and are not our focus in this paper.)

Previous theories

The structure of polymeric crystal-melt interfaces has long been a challenge to theory. A generation ago, there was spirited debate over how amorphous polymer chains emerging from a crystalline lamella reentered the lamella at some other location. The contending views were the “adjacent reentry” model, which held that emerging chains predominately formed tight loops and re-entered the crystal right next to where they exited;⁴ and the “switchboard” model, which said that emerging chains made fluffier, more random loops and typically re-entered the crystal at distant locations.^{5,6}

Attempts were made to compute conformational probabilities for the amorphous chain loops at the crystal-melt interface, but they suffered from various shortcomings.

Either chain connectivity was not properly respected,^{7–12} or the constraint of constant melt density was not enforced, in so-called “Gambler’s Ruin” models of noninteracting chains at interfaces.^{13–15} Models of the Gambler’s Ruin type have been used more recently to study crystallization of single chains in solution,¹⁶ and the shapes of single crystals composed of many chains.¹⁷ But these works share all the shortcomings of their antecedents — they assume noninteracting, fully flexible, Gaussian chains — and so can only qualitatively describe the melt-crystal interface.

More recently, Monte Carlo simulation techniques have been fruitfully applied to study the melt-crystal interface.^{18–20} These united-atom simulations give detailed information on chain conformations, internal stresses, and potential energies of an equilibrium interface. However, these simulations are not able to predict interfacial free energies, a key parameter in nucleation theory, discussed below.

Considerable work has also been done on the properties of grafted polymers at interfaces — “polymer brushes”.^{21–23} In this paper, I will use the modern theory of polymer brushes to provide a definitive theory of the crystal-melt interface. With this theory, predictions can be made for the interfacial structure, free energy, fraction of adjacent reentry, and other physical properties of interest.

Nucleation

There is a new reason to be interested in the structure of the polymer melt-crystal interface, which again relates to an old debate, as to the mechanism for nucleation of polymer crystals.

The classical theory of nucleation in an undercooled, metastable liquid phase posits a small ‘nucleus’ — a tiny crystal, that may or may not grow — which comes into existence by random fluctuations.²⁴ (See Fig. 2a.) The driving force for the nucleus to grow is that its free energy is lower than that of the surrounding melt. However, the interface between the nucleus and melt has an interfacial tension, which inhibits growth of small crystals. The free energy as a function of crystal size is the sum of the bulk and surface terms, with a maximum, corresponding to the “critical nucleus”, beyond which further increases in size actually decrease the total free energy.

For a cylindrical nucleus, appropriate to a lamellar crystal, the nucleation barrier is^{25,26}

$$\Delta G^* = \frac{8\pi\gamma_s^2\gamma_e}{(\Delta S\Delta T)^2} \quad (1)$$

in which ΔS is the transition entropy, ΔT the undercooling, and γ_e and γ_s are respectively the interfacial tensions on the “end” and “side” of the cylindrical nucleus.

The question arises: what phase nucleates? The naive answer is, the most stable phase; but Ostwald’s “rule of stages” reminds us that in matters of kinetics, victory belongs to the swift — the phase with the lowest nucleation barrier nucleates first.²⁷ After nucleating, this phase may grow, or convert to the most stable phase. This phenomenon is commonly observed and of great practical importance in metallurgy.

Regarding nucleation in polymers, long ago the suggestion was made that the critical nucleus consisted not of a small polymer crystal, but rather a collection of more-or-less parallel chain segments gathered together from the melt like a sheaf of wheat.²⁸ This hypothetical structure for the critical nucleus, known as a “fringed micelle”, was rebutted by the argument that the fringed micelle would not have a strong bulk driving term (not being a crystal with its favorable free energy), while still having an interface made of stretched and distorted “fringe” chains.^{29–31}

Rotator phases

However, strong evidence has recently accumulated that polyethylene nucleates via a metastable partially ordered phase, called a “rotator” phase.^{32–36} In a rotator phase, chains are parallel, and packed on a regular lattice in the plane normal to the chain direction, but retain some freedom to rotate about their own axes. They therefore have a somewhat lower areal density of chain stems than does the crystal, which will be crucial for this paper. (See Fig. 2b.) Rotator phases are stable in linear alkanes with 25–60 carbons or so (basically short pieces of polyethylene), for a narrow range of temperatures between the crystal and melt phases,³⁷ and are stable at elevated pressures and temperatures in polyethylene.³⁸

The evidence for nucleation via rotator phases in polyethylene is circumstantial, but

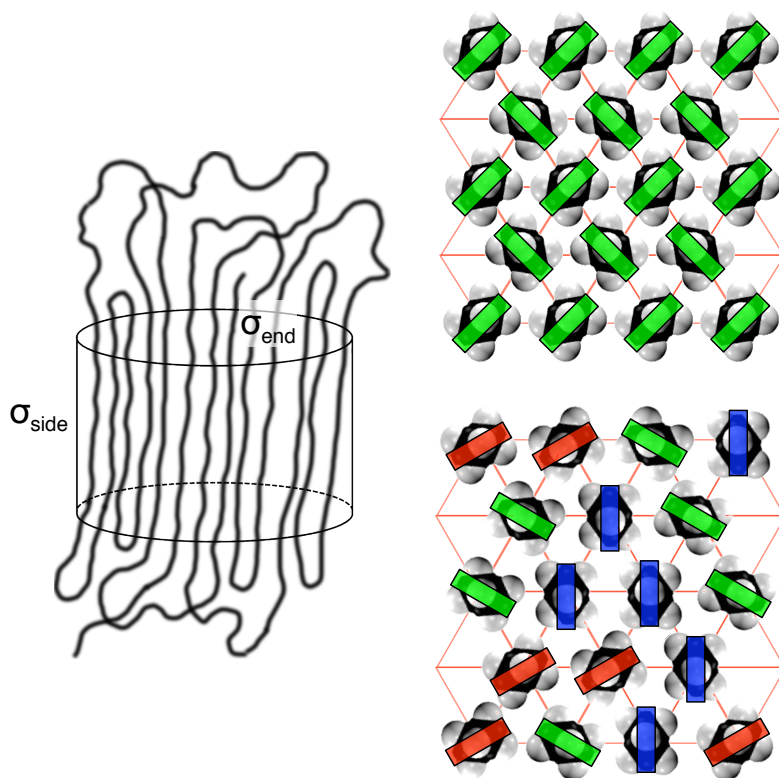


Figure 2: a) Sketch of a nucleus for crystallization, consisting of a cylindrical bundle of parallel chain stems, bounded by a “fringe” of amorphous loops and chain segments into the surrounding melt. b) Top view of the crystalline and rotator RII phases of normal alkanes (oligomeric PE).

quite suggestive. First, time-dependent X-ray scattering in linear alkanes shows that a transient rotator phase appears during a quench into the crystal phase.^{39,40} Second, the quench depth required to achieve a given nucleation rate in linear alkanes shows a smooth dependence on carbon number, only if the quench is assumed to be with respect to the *rotator* phase melting temperature.³⁴

Also, in polyethylene with a bit of comonomer, the comonomer sidechain is known to be rejected from the crystal phase; only uninterrupted ethylene sequences crystallize. Indeed, the melting temperature of such crystals is found to be suppressed by the rejected comonomer, much as the osmotic pressure of salt suppresses the melting temperature of ice (from which the salt is rejected).

This effect is evident in the “melting line” data of Strobl, who presents melting temperature $T_m(d)$ versus lamellar thickness d for a series of ethylene-octene copolymers. The melting line, well described by the Gibbs-Thompson relation

$$T_m(d) = T_m(\infty) - 2\sigma/d\Delta S, \quad (2)$$

is shifted to lower temperatures with increasing octene content.

However: the presence of a bit of comonomer has no effect on the “crystallization line”, which reports the lamellar thickness versus crystallization temperature T_x .^{36,41,42} This suggests a picture in which lamellae nucleated into a mesophase, then thickened (because chains in the mesophase are more mobile) until converting at some larger thickness to the crystal phase. No comonomer effect is observed, because the comonomer was already expelled from the mesophase.⁴³

So the “fringed micelle” idea of polymer nucleation may actually correspond to the current hypothesis that polyethylene, and perhaps other polymers as well, nucleate via rotator phases. In the context of Ostwald’s Rule, rotator phases would be favored to nucleate if they had competitive bulk free energy to that of the crystal (which is suggested by their being stable in a narrow range of temperatures for alkanes), as well as a lower surface tension against the melt than that of the crystal. So to predict what phase nucleates polyethylene, we need a theory for the free energy difference between

rotator and crystal phases, and a theory for the interfacial free energy of both ordered phases against a melt.

New theory for melt-crystal interfaces

Thus we again meet the question, what is the structure and free energy of the interface between an ordered polymer phase (crystal or rotator) and the melt? In the language of grafted polymer brushes, the carpet of amorphous chain loops at the crystal-melt interface is a “pseudobrush”, first studied in the context of adsorbed polymers at interfaces⁴⁴. By pseudobrush, we mean a polydisperse brush of loops, in which the length distribution of the loops is determined not by a chemist but by the system itself, as it seeks to minimize its free energy subject to constraints.

For the crystal-melt interface pseudobrush, the constraints are 1) constant local “melt” density in the amorphous region, and 2) an areal density of “injected” chains emerging from the crystal set by the crystal structure (which we regard as unperturbed by the interface). Subject to these constraints, the system determines the best loop-length distribution, that maximizes configurational entropy and minimizes chain bending. That is, the system must resolve the “crowding paradox”: the injected chains are at much too high an areal density to make random walks in the amorphous region — if they did so, they would overflow space. So some of the chains must make tight loops (which cost bending energy) to reenter the lamella, so that other chains may take more nearly random configurations to gain entropy, and thus interpolate between the strongly oriented chains of the ordered phase, and an isotropic melt region well above.

To simplify the theorist’s task, we make the following assumptions:

- Chains of infinite length (no free ends);
- Semi-infinite melt region above the crystalline lamella (only one interface);
- Interface in equilibrium at the melting point (can use equilibrium statistical mechanics).

These assumptions may seem at cross purposes with studying nucleation — infinite-length chains will take forever to equilibrate, and how will the results be relevant to the formation and growth kinetics of a critical nucleus? However, our equilibrium estimate will be a lower bound on the interfacial tension of an incompletely equilibrated structure; as well, we can argue that the residual effects of distant large loops on the interfacial free energy will be minimal. Free end effects are a small perturbation in a typical high molecular weight polymer sample; tie chains are likewise a small perturbation, since estimates from Gumbler’s Ruin models indicate that only a few percent at most of stems give rise to tie chains.

Self-consistent field theory

We use self-consistent field theory to describe melts of polymer chains in inhomogeneous environments, such as for chains attached to an interface.^{21–23} In SCFT, we consider each chain to interact with others only through the hydrostatic pressure field, which is adjusted (self-consistently) to enforce the constraint of constant melt density. For a end-grafted polymer layer or “brush” at reasonably high coverage (chains per area), the hydrostatic pressure is high near the grafting surface, to drive the chains to stretch and thereby avoid overfilling space near the surface.

In cases where chains are “strongly stretched” well beyond their random-coil dimensions, elegant analytical approximations exist for calculating chain conformations, pressure profiles, and interfacial free energies.^{44–46} However, for the crystal-melt interface, we expect that many of the loops will be quite short, and so the analytical strong-stretching approach would not be valid.

There are several equivalent formulations of SCFT,⁴⁷ but for present purposes the simplest is to consider chains on a semi-infinite simple cubic lattice, with the crystal face as boundary. The lattice version of SCFT has the advantage of naturally imposing a short-distance “monomer cutoff”. (Bending energies can also be easily added, as we shall see below.) Lattice SCFT is particularly tractable in problems such as a grafted layer, in which the potential only varies in one dimension.

Of course, we may consider pseudobrushes at different coverages. One important

limit corresponds to the pseudobrush we form by cutting with a plane an isotropic melt of infinite-length chains. Each half-space forms a pseudobrush of polydisperse loops, in this case with constant hydrostatic pressure, so that the loops are isotropic random walks above an absorbing boundary. The coverage for this pseudobrush on a simple cubic lattice is $1/6$, since for all the lattice sites adjacent to the boundary plane, the probability for the chain passing through there to be headed across the plane is $1/6$. (This is true even for semiflexible chains, for which bends are penalized.) The isotropic pseudobrush should be the minimum free energy state, since it corresponds to unconstrained chains.

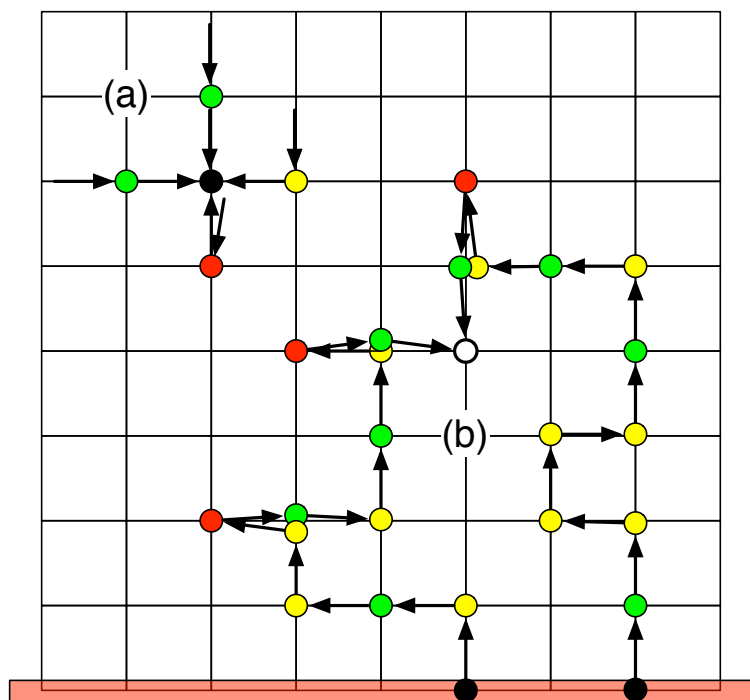


Figure 3: a) Cartoon of lattice SCFT evolution; for a chain path to arrive at the central point (dark circle) on the j th step, it must have come from a neighboring site on the previous step. b) The density at a given point (open circle) is the Boltzmann-weighted sum over all paths passing through the point. Colors denote straight paths (green), bends (yellow), backfolds (red).

SCFT consists of the following elements (see Fig. 3):

1. make an initial guess for the self-consistent pressure potential U_k on the k th layer;

2. given U_k , compute the Boltzmann weight $P(k, j)$ (single-chain partition function) for a chain segment starting from the crystal surface to reach the k th lattice layer in j steps;
3. compute the monomer density ρ_k on the k th layer (by summing over all paths through that layer, each weighted by its Boltzmann weight);
4. adjust U_k until the density constraint (constant ρ_k on each layer) is satisfied.

(See Appendix for details.)

Surprisingly, only the potential in the first layer is appreciably nonzero — U_k for $k > 1$ are smaller by a factor of typically 100 or more, and oscillatory functions of k . This result suggests *assuming* that a nonzero value of U_1 is all that is required to achieve a self-consistent solution everywhere above the lamella. Then, an arbitrary chain trajectory in the self-consistent potential would consist of a sequence of “trains” (random walks in the first layer only) and “free loops” into layers 2 and above. (See Fig. 4a.) Because the potential $U_{k>1}$ is assumed zero, the free loops would indeed be isotropic random walks above an absorbing boundary; i.e., the same configurations of loops as in the isotropic melt pseudobrush.

Upon reflection, it is evident that one more constraint parameter is required; namely, a Lagrange multiplier to control the injection density into layers 2 and above. The single parameter U_1 cannot control both the melt density in layer 1, and also the injection density into the space above. One may say that this multiplier takes care of what those small oscillatory values of $U_{k>1}$ were doing in the numerical SCFT calculation. With this addition, it turns out to be possible to enumerate chain configurations exactly; the Boltzmann weight for a train is a geometric series. Likewise, a sequence of trains and loops results in a geometric series.

After considerable algebra, a startlingly simple formula emerges for the free energy per loop $F(\sigma)$ as a function of loops per area σ :

$$\begin{aligned}
 F/L &= \left(\frac{5}{6\sigma} - 1 \right) \log \left(\frac{5}{4} - \frac{3\sigma}{2} \right) + \log \sigma \\
 U_1 &= -\log [(5/4)(1 - 6\sigma/5)]
 \end{aligned} \tag{3}$$

The free energy per loop (see Fig. 4, lowest dark curve) shows the expected minimum at the coverage $\sigma = 1/6$, which corresponds to the isotropic melt pseudobrush. For $\sigma > 1/6$, the potential U_1 tends to drive monomers out of the first layer, while for $\sigma < 1/6$ it tends to draw them in. Note that the maximum possible coverage for flexible chains is $\sigma = 5/6$; at this coverage, on average for every six surface sites, four injected chains have the tightest possible loop (one backfold) and one makes a free loop in the space above the first layer.

Bending stiffness

Of course, real chains have bending stiffness; on the lattice, 90 degree bends and backfolds (180 degree bends) should come at a price. Fortunately, this can be incorporated into the lattice SCFT in a straightforward manner. For semiflexible lattice chains, it suffices to compute the Boltzmann weight $P(k, t, j)$ for a chain to arrive at layer k pointed in direction t (either up, down, or horizontal) after j steps from the grafting surface.

Again, we can numerically solve the lattice SCFT equations for semiflexible chains. (See Appendix for details.) And again, we find the surprising result that the self-consistent potential is essentially only one layer deep. And so we are again motivated to assume this is so (and as before, we use a Lagrange multiplier to control the injection density of free loops into layer 2 and above).

Amazingly, even for semiflexible chains it turns out to be possible to enumerate the relevant Boltzmann weights exactly, by summing over chain configurations as sequences of trains and free loops. (However, the resulting equation for the constraint potential U_1 must be solved numerically, so analytical expressions for the free energy per loop cannot be given.)

The semiflexible model has two parameters describing the bending penalties; namely, the Boltzmann weights $b = \exp(-\beta \epsilon_b)$ for a 90 degree bend, and $B = \exp(-\beta \epsilon_B)$ for a 180 degree backfold. The resulting free energy per loop, for various values of b and B , is displayed in Fig. 4. The upper set of curves correspond to $B = 0$ (no backfolds allowed) and increasing values of b from top to bottom, with $b = 1$ (no cost for 90 degree bend) as the last curve in the set. The lower set of curves correspond to $b = 1$

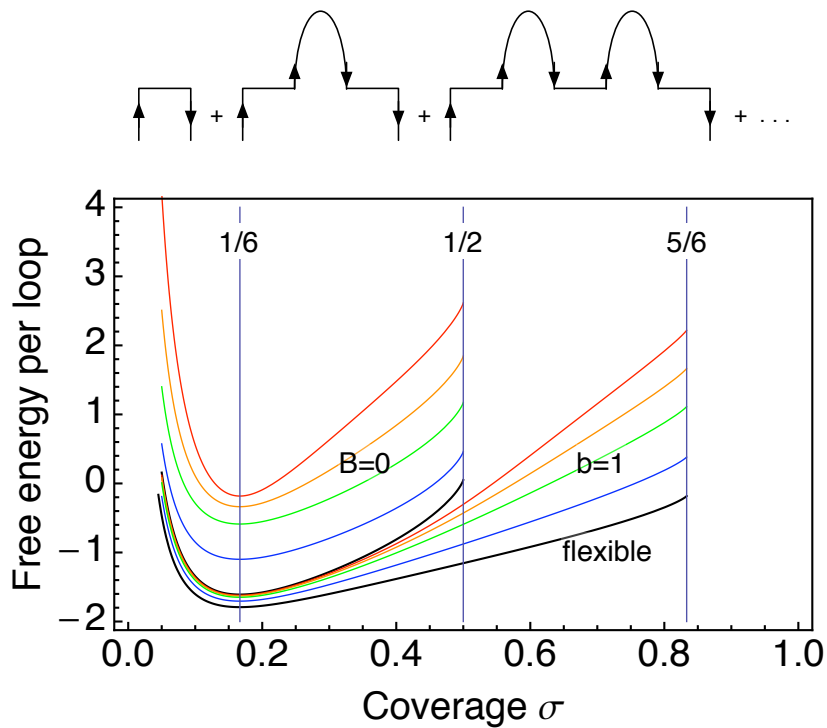


Figure 4: a) General trajectory for a loop as a sequence of “trains” in the first layer, separated by “free loops” in the layers above (where $U = 0$). b) Free energy per loop, for various values of b and B . The lowest curve is the flexible limit, Eqn. (3). Immediately above, $b = 1$ (no cost for 90 degree bend) and $B = 0.5, 0.2, 0.1, 0.05$ (progressively stiffer backfolds). Middle dark curve is $b = 1, B = 0$ (no backfolds); above are $B = 0$ and $b = 0.5, 0.2, 0.1, 0.05$ (progressively stiffer 90 degree bends).

and increasing values of B from top to bottom, with $B = 1$ (flexible limit) as the last curve.

Note that if B is strictly zero, the maximum injection density is $\sigma = 1/2$, for which we have on average on every six surface sites, two chains injected making a tight loop (two 90 degree bends and out), and one chain making a free loop in the space above.

Putting polymers on a lattice

To make contact with experiment, we map real polyethylene chains onto a lattice, as follows. We choose a monomer to be two CH_2 groups, and the cell volume to be the volume of this monomer in a real melt at 145C (about 59.5 \AA^3). One gauche bond in a chain gives rise to a 60 degree bend, and two gauche bonds in succession gives a 90 degree bend, so our monomer is able to make a 90 degree bend. (The reason for taking a somewhat finer lattice than usual, corresponding to two monomer units rather than an entire Kuhn length, is so that the important effects of bending stiffness and finite extensibility can be incorporated into the lattice description.) The resulting cell linear dimension is then 3.9 \AA .

We forbid backfolds for steric reasons, and so set $B = 0$. We choose b so that the mean-square end-to-end distance of chains on the lattice, given by

$$\frac{R^2}{N} = a^2 \left(\frac{1 + 4b + B}{4b + 2B} \right) \quad (4)$$

matches the value for real melt polyethylene (about $1.25 \text{ \AA}^2/(\text{g/mol})$).⁴⁸ This gives $b = 0.192$ or $\epsilon_b = 5.7 \text{ kJ/mol}$ at 145C; this value is a bit lower than twice the trans-gauche energy difference (of about 3 kJ/mol), but one can argue that short-distance fluctuations renormalize the naive value downwards.

The area per stem in the crystal phase is about 18.5 \AA^2 , which is a bit larger than the plaquette size in our lattice model. However, we insist that the areal density of injected chains from the crystal (half the areal density of chain stems) must correspond to the maximum coverage $\sigma = 1/2$. The argument for this identification is as follows: if we injected chains at exactly twice this density, there would be no freedom whatsoever —

the chains would be obliged to be completely straight, which would correspond to a continuation of the crystal.

Amorphous-phase tension; interfacial tilt

Real crystal-melt interfaces in polyethylene are commonly observed to be tilted with respect to the plane normal to the chain stems. The most frequently observed interface is around [201], at about 34 degrees off normal.¹ Intuitively, the interface tilts to relieve crowding of the chains entering the melt region; but what limits the degree of tilt?

To take advantage of the reduced crowding afforded by a tilted interface, the chains must bend as they cross the interface (so that they enter the melt region in the normal direction). We model the bending cost as quadratic in the angle, with a magnitude determined by the observation that at an inclination of 60 degrees, every stem crossing the surface would require one gauche bond.

With this prescription, we can minimize the free energy per loop with respect to the interfacial tilt angle, and find the optimum tilt angle and corresponding interfacial free energy per area. The results are in encouraging agreement with the common occurrence of [201], also seen in atomistic simulations of PE.¹⁹ We find an optimum tilt angle of 34 degrees, and a corresponding interfacial tension contribution (with respect to the base area) of 22.2 mN/m, or about 1.5 kT per loop. The fraction of adjacent reentry (defined for the lattice model as injected chains that immediately make two 90 degree bends and reenter the lamella) is found to be 0.38, in good agreement with simulations.¹⁸

Using our methods, the interface between a lamellar region of RII rotator phase and the adjacent melt can be considered as easily as the crystal-melt interface. The only difference between the two is a lower injection density of chains, lower by a factor 18.25/21, the ratio of chains per area in the two ordered phases. But because the crystal is so crowded, corresponding to the maximum possible injection density ($\sigma = 1/2$), the effect of a small increase in area per chain is significant. We find that, in contrast to the crystal-melt interface, the RII-melt interface occurs at essentially zero tilt angle, with an interfacial tension almost 40 percent lower — 14.7 mN/m versus 23.7 mN/m for the crystal.

We can also treat the interfacial free energy cost of the “side” of a crystal lamella adjacent to melt. Indeed, this corresponds to the limit of zero injected chain density, simply an impenetrable boundary from which isotropic chains are repelled. In this case, the contributions is computed to be 10.1 mN/m and 8.9mN/m for the crystal and rotator phases respectively.

Additional contributions to σ

So far, we have focused on the interfacial free energy of the amorphous loops. There are three additional contributions to the interfacial tension of the end and side faces, from 1) disruption of crystalline order by randomly reentrant loops on the end faces; 2) missing ordered-phase neighbors on the side faces; and 3) dispersive interactions between phases of different density. In all three cases, the contribution for rotator-melt interfaces is smaller than for crystal-melt interfaces, because the the enthalpy and density differences with respect to the melt are smaller for the rotator phase than for the crystal phase. (See Appendix for details).

The most important of these contributions is the interfacial free energy associated with disruption of crystalline periodicity, at the interface in proximity to the amorphous region. Atomistic Monte Carlo simulations of the Rutledge group²⁰ show that on the crystalline side of the interface (as defined by the density variation) the crystalline order is disrupted.

The potential energy rises sharply with a tanh-like profile, with a width of about 1.6Å the height of a monomer or so in the all-trans configuration (see Figs. 3 and 4 of Ref.²⁰). We model this interfacial free energy arising from disordering the crystal using Cahn-Hilliard theory, with parameters from Ref.²⁰ and experiment (see Appendix for details).

Table 1 reports the computed values for all contributions to the melt interfacial tensions of rotator (R) and crystal (X) phases, on end and side faces: “xtal” are from disruption of order (end) or missing neighbors (side); “melt” are from free energy of amorphous loops (end or side, treated in the previous sections); “vdW” are from dispersive interactions.

phase	end				side				spherical	expt.	
	xtal	melt	vdW	Total	xtal	melt	vdW	Total	$(\sigma_e \sigma_s^2)^{1/3}$	$(\sigma_e \sigma_s^2)^{1/3}$	σ_e
R	18.3	14.7	0.2	33.1	7.3	8.9	0.2	16.4	20.7	23.5	—
X	32.0	23.7	1.4	57.1	13.0	10.1	1.4	24.5	32.5	37.7	54.6

Table 1: Calculated contributions to end and side interfacial tension σ_e and σ_s for rotator (R) and crystal (X) phases, and “spherical average” $(\sigma_e \sigma_s^2)^{1/3}$; experimental values for spherical average and σ_e , described in text.

There are no direct experimental values for any of the interfacial tensions, except the end-face crystal-melt tension $\sigma_{XL}^{(e)}$, obtained from the slope of the Gibbs-Thompson melting line.³⁶ Remarkably, the measured value is within 5% of the computed result (see Table 1). This agreement affords a small measure of confidence in our other interfacial tension values.

Nucleation barriers

With values for the various interfacial tensions in hand, we set about estimating the barriers to nucleation via rotator and crystal phase nuclei. For this purpose, we require values for the transition temperatures T_{XL} and T_{RL} and transition entropies ΔS_{XL} and ΔS_{RL} (X = crystal, R = rotator RII, L = liquid).

The transition entropies ΔS_{XL} and ΔS_{RL} are available from calorimetry experiments on linear alkanes in the range C₂₀–C₆₀.³⁴ The values of ΔS_{XL} and ΔS_{RL} depend on carbon number n , but settle down by $n = 35$ or so to essentially constant values of 0.718J/(g K) and 0.485J/(g K) respectively. We obtain $T_{XL} = 145\text{C}$ by extrapolating the “melting line” ($T_{XL}(d)$ versus lamellar thickness $1/d$).³⁶

T_{RL} is more problematic, since rotator phases are only metastable in polyethylene at standard pressure. Values from the alkane series have significant n -dependence even at $n = 60$, and extrapolation to $n = \infty$ is not unambiguous. Instead, we make use of the value for T_{XR} of 158C, from extrapolating the crystallization line to infinite lamellar thickness.³⁶ Then, because the transition temperatures $T_{RL} < T_{XL} < T_{XR}$ are all close, we determine T_{RL} from a linear approximation on the free energy difference ΔF_{XR} ,

$$\Delta F_{XR} = \Delta F_{XL} - \Delta F_{RL} = (T - T_{XL})\Delta S_{XL} - (T - T_{RL})\Delta S_{RL} \quad (5)$$

and the requirement that $\Delta F_{XR} = 0$ at $T = T_{XR}$, which fixes the value of $T_{RL} = 139\text{C}$.

Now, using Eqn. (1) we can compute ΔG^* as a function of temperature, assuming nucleation via rotator or crystal phase. The result (see Fig. 5) is satisfying: the barrier is lower for nucleation via rotator, for temperatures lower than about 115C . Nucleation theory also predicts the area and thickness of the critical nucleus,³⁴ shown in the inset to Fig. 5. Above 115C , both barriers increase sharply, and indeed nucleation is essentially unobservable at such shallow undercoolings in PE. The rotator phase wins out both because its interfacial tensions are lower, and because it is nearly stable, with T_{RL} only 6C below T_{XL} .

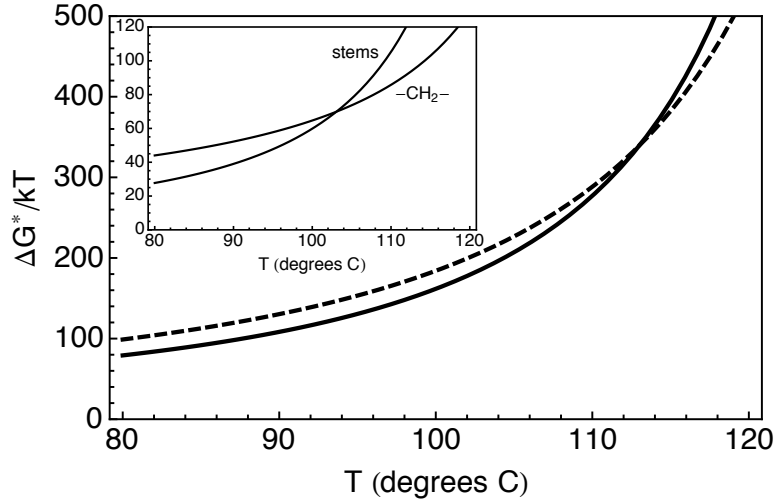


Figure 5: Barriers for nucleation via rotator (solid) and crystal nuclei. Inset: number of stems and CH_2 groups.

Our nucleation theory can also be compared to results of Ross and Frolen, who measured homogenous nucleation rates in PE.⁴⁹ Their data can be compared to the classical prediction for the nucleation rate,

$$\log I(T) = \log K_V - D/(T\Delta T^2) \quad (6)$$

in which the slope D on a plot of $\log I(T)$ versus $1/(T\Delta T^2)$ is predicted to be

$$D = \frac{8\pi\sigma_e\sigma_s^2}{k\Delta S^2} \quad (7)$$

Thus, a value for $(\sigma_e \sigma_s^2)^{1/3}$ can be extracted from the Ross-Frolen data, if one assumes the critical nucleus to be either crystal or rotator phase (therefore determining the appropriate values of ΔS and ΔT). Table 1 reports best-fit values for $(\sigma_e \sigma_s^2)^{1/3}$ under both assumptions, in which the log attempt frequency $\log K_v$ was also fitted. The Ross-Frolen data itself is not sufficient to distinguish which phase nucleates, but it is noteworthy that the inferred interfacial tension values for nucleation via rotator phase are within 13% of our predictions. Finally, the fitted attempt frequency, long estimated to be the vibrational time of a Kuhn segment (about $10^{34}/\text{sec}$),⁴⁹ is “only” 10^3 times this nominal value assuming rotator phase nucleation, but is fitted to be nearly 10^8 times larger if we assume nucleation via crystal.

Rotator phases may be operative in the crystallization of other polymers as well. The characteristic behavior of the melting and crystallization lines seen by Strobl for PE is repeated in data for isotactic and syndiotactic polypropylene.^{36,50} Ordered packings of parallel stems (all-trans, or helical) are a common feature of polymer crystals, and these stems could rotationally disorder in a fashion similar to PE. Rotator phases are only well known in PE because of studies on alkanes; oligomers of other polymers can also be studied experimentally or simulated to look for metastable rotator phases, a subject of continuing work in our group. It may be that some aspects of the present approach could also be relevant to crystallization of colloidal particles or proteins, where densely packed but rotationally disordered mesophases may also play an important role in nucleation.

Acknowledgements: I thank Eric Sirota, Gert Strobl, and Elie Raphael for useful discussions, and the Laboratoire “GULLIVER” at the Ecole Supérieure de Physique et de Chimie Industrielles de la Ville de Paris (ESPCI) for their hospitality during which a portion of this work was carried out. This work was supported in part by NSF DMR-0907370.

Appendix

Self-consistent field theory, flexible case.

The equations that implement this procedure are

$$\begin{aligned} P(k, n+1) &= (1/6) [P(k-1, n) + 4P(k, n) + P(k+1, n)] \exp(-U_k) \\ P(k, 1) &= \delta_{k,1} \end{aligned} \quad (8)$$

$$\begin{aligned} \delta\rho(k, n) &= \exp(U_k) \sum_j P(k, j) P(k, n-j) \\ \rho(k) &= \sigma \sum_n \frac{nP(n)\delta\rho(k, n)}{\sum_k \delta\rho(k, n)} \end{aligned} \quad (9)$$

The normalization of the Boltzmann weights so calculated is such that free chains have a Boltzmann weight of unity.

Here we have introduced loop length distribution $p(n)$, the probability that an injected chain will form a loop of length n . The loop length distribution for the crystal-melt interface is determined to minimize the free energy per loop F , given by

$$F/L = - \sum_n p(n) \log P(1, n) + \sum_n p(n) \log p(n) - (1/\sigma) \sum_k U_k \quad (10)$$

The first term is the $p(n)$ -weighted average of the free energy (log of the partition function) for a loop of length n ; the second is the Shannon entropy of the loop length distribution itself. [The third term subtracts the (artificial) work done by the constraint potential.] Minimizing over $p(n)$ gives the reasonable result that $p(n)$ is proportional to the Boltzmann weight for loops of length n .

The resulting numerical procedure can be carried out for a melt-crystal interface at different values for the “injection density” (areal density of chains emerging from the lamella). (Practically, the self-consistent potential U_k is computed stepwise, by enforcing the density constraint on only the first layer using only U_1 , then on the first two layers using only U_1 and U_2 , and so forth, each time using the previous result for

U_k as the initial guess.)

Semiflexible case

In terms of the Boltzmann weight $P(k, t, j)$, the generalized SCFT equations can be written

$$\begin{aligned}
P(k, +, n+1) &= C[P(k-1, +, n) + bP(k-1, 0, n) + BP(k-1, -, n)] \exp(-U_k) \\
P(k, 0, n+1) &= C[(1+2b+B)P(k, 0, n) + 4bP(k, +, n) + 4bP(k, -, n)] \exp(-U_k) \\
P(k, -, n+1) &= C[P(k+1, -, n) + bP(k+1, 0, n) + BP(k+1, +, n)] \exp(-U_k) \\
C &= 1/(1+4b+B)
\end{aligned} \tag{11}$$

with corresponding expression for the density

$$\rho(k, n) = \exp(U_k) \sum_{m=1}^n \sum_{t_1, t_2} P(k, t_1, m) P(k, t_2, n-m) M_{t_1 t_2} \tag{12}$$

with t_1 and t_2 taking on the values $+, -, 0$, and the coupling matrix M given by

$$M = \begin{bmatrix} B & b & 1 \\ b & (1+2b+B)/4 & b \\ 1 & b & B \end{bmatrix} \tag{13}$$

In the above, $b = \exp(-\beta \varepsilon_b)$ and $B = \exp(-\beta \varepsilon_B)$ are respectively the Boltzmann factors for a 90 degree bend and a backfold. (See Fig. 3.)

“Disordering” contribution to interfacial tension

We model this interfacial free energy arising from disordering the crystal using Cahn-Hilliard theory. We write an effective free energy per unit interfacial area as

$$\beta F/A = (1/v) \int dz \left(\frac{a^2}{2} \left(\frac{\partial \psi}{\partial z} \right)^2 + 16b\psi^2(1-\psi)^2 \right) \tag{14}$$

Here v is a monomeric volume, a is a characteristic length, and ψ is the order parameter (e.g., the strength of the density wave). The second term is the usual quartic double-well potential, with minima at $\psi = 1$ (ordered state) and at $\psi = 0$ (disordered state). At the equilibrium melting point, the two states have equal free energy. The height of the double-well barrier is b , which is the free energy cost at $\psi = 1/2$, “halfway between” the ordered crystal and disordered state.

The Cahn-Hilliard solution gives the order parameter profile $\psi(z)$ as a tanh,

$$\psi(z) = (1/2) \left(1 + \tanh(4\sqrt{2b}z/a) \right) \quad (15)$$

with a width $w = a/(4\sqrt{2b})$, which we set equal to 1.6\AA . The interfacial free energy is

$$\beta F/A = 16bw/(3v) \quad (16)$$

The free energy density at the interface midpoint is $b/(4v)$, so $\beta F/A$ equals $(4/3)f_{max}w$, scaling as the maximum free energy density penalty times the width. We make a guess for the “barrier height” (free energy value at $\psi = 1/2$), that it is half as big as the maximum possible value, i.e., half the transition enthalpy. (The maximum barrier would obtain if the intermediate state had none of the energy reduction of the ordered phase, and none of the entropy gain of the ordered phase.)

With values for transition enthalpies and temperatures as described in the main text, and densities of 0.99g/cm^3 and 0.91g/cm^3 for crystal and rotator phases, the resulting energy densities are 300J/cm^3 and 171J/cm^3 respectively. We assume the interfacial widths to be the same for the crystal and rotator interfaces, namely $w = 1.6\text{\AA}$, and take v to be the volume of a monomer in the ordered phase. Applying these results gives the disordering contributions to σ_{end} of Table 1.

On the sides of the nucleus, crystalline order terminates abruptly, without the disordering effect of returning chains. Here, a sensible estimate of the short-range contributions to interfacial energy is to say that bonds to missing ordered-phase neighbors on the surface are “broken”. The interfacial energy cost is the formation enthalpy per CH_2 group, divided by the surface area of a cell containing one CH_2 group, times the frac-

tion of cell area associated with missing neighbors. This procedure gives contributions reported in Table 1.

Dispersive contribution to interfacial tension

The density of the melt (about 0.845g/cm³) at room temperature is slightly lower than that of the crystal (about 1.0g/cm³).⁵¹ Thus, the density of polarizable groups giving rise to dispersive forces, and hence the Hamaker constant, would be larger in the crystal than the melt. The rotator phase has a density we estimate from the ratio of areal densities for crystal and rotator, as 18.5/21 times 1g/cm³, or about 0.9g/cm³.

The Hamaker constant can be well estimated from the index of refraction using an approximation to the full Lifshitz theory of dispersive interactions:⁵²

$$A \approx \frac{3h\nu_e}{16\sqrt{2}} \frac{(n_1^2 - n_2^2)^2}{(n_1^2 + n_2^2)^{3/2}} \quad (17)$$

in which ν_e is a typical optical absorption frequency of about 3×10^{15} Hz, n_1 and n_2 are the indices of refraction of the two phases.

The difference in index of refraction between crystal and melt can be obtained from the Clausius-Mossotti relation,⁵³

$$\frac{n^2 - 1}{n^2 + 2} \propto \rho \quad (18)$$

The dispersive contribution to interfacial tension is then given by an integral of the dispersive forces between two slabs of material A (crystal) interacting across a slab of material B (melt), comparing results at large separations and at a short-distance cutoff of about 1.5Å:⁵²

$$2\gamma = \frac{A}{12\pi D_0^2} \quad (19)$$

We find for liquid normal alkanes interacting across air, a value of $A_{232} = 6.59 \times 10^{-20}$ J (1 = ordered, 2 = liquid, 3 = air), and for solid normal alkanes interacting across liquid normal alkanes, a value of $A_{121} = 2.80 \times 10^{-21}$ J. Assuming the cutoff distance

is the same in the two cases, the interfacial tension γ_{12} is then

$$\gamma_{12} = \gamma_{23} \frac{A_{121}}{A_{232}} \quad (20)$$

Alkane interfacial tensions against air at 20C, extrapolated to high molecular weight, gives $\gamma_{23} = 33.5$ dyn/cm. Applying these results gives the values labeled “vdW” in Table 1.

References

- [1] B. Wunderlich, *Macromolecular Physics Vol. 2: Crystal Nucleation, Growth, Annealing*, Academic Press: London, 1976.
- [2] P. Phillips and B. Edwards, *J Polym Sci Pol Lett*, 1976, **14**, 449–454.
- [3] E. Fischer, K. Hahn, J. Kugler, U. Struth, R. Born and M. Stamm, *J Polym Sci Pol Phys*, 1984, **22**, 1491–1513.
- [4] *Treatise on solid state chemistry*, ed. N. Hannay, Plenum Press, New York, 1970, ch. 6–7.
- [5] D. Yoon and P. Flory, *Polymer*, 1977, **18**, 509–513.
- [6] P. Flory and D. Yoon, *Nature*, 1978, **272**, 226–229.
- [7] D. Yoon and P. Flory, *Macromolecules*, 1984, **17**, 868–871.
- [8] P. Flory, D. Yoon and K. Dill, *Macromolecules*, 1984, **17**, 862–868.
- [9] J. Marqusee and K. Dill, *Macromolecules*, 1986, **19**, 2420–2426.
- [10] S. Kumar and D. Yoon, *Macromolecules*, 1989, **22**, 3458–3465.
- [11] J. Marqusee, *Macromolecules*, 1989, **22**, 472–476.
- [12] S. Kumar and D. Yoon, *Macromolecules*, 1989, **22**, 4098–4101.
- [13] E. DiMarzio and C. Guttman, *Polymer*, 1980, **21**, 733–744.

- [14] C. Guttman, E. DiMarzio and J. Hoffman, *Polymer*, 1981, **22**, 1466–1479.
- [15] C. Guttman and E. DiMarzio, *Macromolecules*, 1982, **15**, 525–531.
- [16] M. Muthukumar, *Philos T Roy Soc A*, 2003, **361**, 539–554.
- [17] J. Sommer, *Eur Phys J E*, 2006, **19**, 413–422.
- [18] S. Balijepalli and G. Rutledge, *Comput Theor Polym S*, 2000, **10**, 103–113.
- [19] S. Gautam, S. Balijepalli and G. Rutledge, *Macromolecules*, 2000, **33**, 9136–9145.
- [20] M. Hutter, P. J. in 't Veld and G. C. Rutledge, *Polymer*, 2006, **47**, 5494–5504.
- [21] J. Scheutjens and G. Fleer, *J Phys Chem-Us*, 1979, **83**, 1619–1635.
- [22] T. Cosgrove, T. Heath, B. vanLent, F. Leermakers and J. Scheutjens, *Macromolecules*, 1987, **20**, 1692–1696.
- [23] S. Milner, *J Chem Soc Faraday T*, 1990, **86**, 1349–1353.
- [24] D. Turnbull and R. Cormia, *J Chem Phys*, 1961, **34**, 820–&.
- [25] D. Uhlmann, G. Kritchevsky, R. Straff and G. Scherer, *J Chem Phys*, 1975, **62**, 4896–4903.
- [26] M. Oliver and P. Calvert, *J Cryst Growth*, 1975, **30**, 343–351.
- [27] W. Ostwald, *Z. Phys. Chem.*, 1987, **22**, 289–.
- [28] P. Flory, *J Am Chem Soc*, 1962, **84**, 2857–&.
- [29] H. Zachmann, *Kolloid Z Z Polym*, 1969, **231**, 504–&.
- [30] J. Lauritzen and E. DiMarzio, *J Res Nat Bur Stand*, 1978, **83**, 381–385.
- [31] C. Guttman, E. DiMarzio and J. Hoffman, *J Res Nat Bur Stand*, 1980, **85**, 273–282.
- [32] S. Rastogi, M. Hikosaka, H. Kawabata and A. Keller, *Makromol Chem-M Symp*, 1991, **48-9**, 103–114.

- [33] S. Rastogi, M. Hikosaka, H. Kawabata and A. Keller, *Macromolecules*, 1991, **24**, 6384–6391.
- [34] H. Kraack, M. Deutsch and E. Sirota, *Macromolecules*, 2000, **33**, 6174–6184.
- [35] H. Kraack, E. Sirota and M. Deutsch, *Polymer*, 2001, **42**, 8225–8233.
- [36] G. Strobl, *Eur Phys J E*, 2000, **3**, 165–183.
- [37] E. Sirota, *Langmuir*, 1997, **13**, 3849–3859.
- [38] G. S. Ross and L. J. Frolen, *Methods of Experimental Physics*, 1977, **16B**, 339–397.
- [39] E. Sirota and A. Herhold, *Polymer*, 2000, **41**, 8781–8789.
- [40] E. Sirota and A. Herhold, *Science*, 1999, **283**, 529–532.
- [41] M. Grasruck and G. Strobl, *Macromolecules*, 2003, **36**, 86–91.
- [42] M. Al-Hussein and G. Strobl, *Macromolecules*, 2002, **35**, 1672–1676.
- [43] E. B. Sirota, *Macromolecules*, 2007, **40**, 1043–1048.
- [44] M. Aubouy, O. Guiselin and E. Raphael, *Macromolecules*, 1996, **29**, 7261–7268.
- [45] S. Milner, T. Witten and M. Cates, *Macromolecules*, 1989, **22**, 853–861.
- [46] S. Milner, *Science*, 1991, **251**, 905–914.
- [47] M. Matsen and M. Schick, *Physical Review Letters*, 1994, **72**, 2660–2663.
- [48] L. Fetters, D. Lohse, D. Richter, T. Witten and A. Zirkel, *Macromolecules*, 1994, **27**, 4639–4647.
- [49] G. Ross and L. Frolen, *J Res Nbs A Phys Ch*, 1975, **79**, 701–711.
- [50] M. Iijima and G. Strobl, *Macromolecules*, 2000, **33**, 5204–5214.
- [51] *Polymer Handbook*, ed. J. Brandrup, E. Immergut and E. Grulke, Wiley: New York, 4th edn., 1999, pp. VI–8.

- [52] J. Israelachvili, in *Intermolecular and Surface Forces*, Elsevier Academic Press:
London, 1992, ch. 11.
- [53] J. Jackson, in *Classical Electrodynamics*, Wiley: New York, 1975, ch. 4.